Supporting Information

Promoting water formation in sulphate-functionalized Ru for efficient hydrogen oxidation reaction under alkaline electrolyte

Chaoyi Yang, Yunbo Li, Jianchao Yue, Hengjiang Cong, and Wei Luo*

Experimental Procedures

Reagents and materials

Ruthenium (III) acetylacetonate [Ru(acac)$_3$, ~98%, Wuhan, Changcheng Chemical Co., Ltd.], Sulfur [S, >99.99%, China, Sinopharm Chemical Reagent Co., Ltd], potassium bromide [KBr, ~95%, China, Sinopharm Chemical Reagent Co., Ltd.], ethanol and isopropanol [>99% and ~99.5%, China, Sinopharm Chemical Reagent Co., Ltd.], nafion solution [5%, Sigma-Aldrich]. Support: carbon black (Vulcan, XC-72R). The water used in all experiments was prepared by passing through an ultra-pure purification system.

Synthesis of Ru-SO$_4$ and Ru nanosheet

Typically, 80 mg Ru(acac)$_3$ stirred with 180 mg KBr in 10 ml water and 35 ml ethanol for 30 mins in 30 °C. The blending solvent was dried under vacuum drying oven of 60 °C and then annealed at 270 °C for 90 minutes in air. After washing with water and ethanol for three times and collecting by centrifuging, Ru nanosheet is achieved. Ru-SO$_4$ can be obtained by annealing Ru nanosheet at 250 °C by using excessive sulfur.

Physical characterizations

The Powder X-ray diffraction (XRD) patterns were collected by an obtained on a Bruker D8-Advance X-ray diffractometer with a Cu Kα radiation source (λ = 0.154178 nm). The transmission electron microscopy (TEM) images were performed with FEI Tecnai G20 U-Twin operated at 200 kV. The High-revolution transmission electron microscopy (HR-TEM), energy-dispersive X-ray spectroscopy mapping (EDS) and selected area electron diffraction (SEAD) were recorded on JEOL-2100F. X-ray photoelectron spectroscopy experiments were collected with Thermo Fisher ESCALAB 250Xi using Al Kα radiation source. Inductively coupled plasma atomic emission spectroscopy (ICP-AES) were conducted on a Thermo IRIS Intrepid II XSP atomic emission spectrometer. In-situ electrochemical Raman measurement was performed with a home-designed electrochemical cell and a HORIBA Raman microscope equipped with a 638 nm laser and a 50× objective lens. The grating parameter was 600 (750nm), and the laser intensity was 25%. The catalyst ink was drop-casted on a roughened Au disk electrode. X-ray absorption spectroscopy (XAS) including both X-ray absorption near-edge structure (XANES) and extended X-ray absorption fine structure (EXAFS) at Ru K-edge were collected in total-fluorescence-yield mode at ambient air at the BL14W1 beamline of the Shanghai Synchrotron Radiation Facility (SSRF).

Electrochemical measurements

All the electrochemical measurements were conducted by the CHI 760E electrochemical analyzer (CH Instruments, Chenhua Co., Shanghai, China). The standard three-electrode-system were adopted. Glass carbon electrode (GCE, diameter: 5 mm) with catalysts coating were used as the working electrode. The Hg/HgO electrode (MOE) (in 0.1 M KOH or 1.0 M KOH) and the graphite rod were served as reference electrode in alkaline electrolytes and the counter electrode, respectively. All measured potentials were reported versus the reversible hydrogen electrode (RHE) potential.

To prepare catalyst ink for HOR experiments, 4 mg catalysts were dispersing in 2 ml isopropanol solution containing 0.05% Nafion. The mixture solvent was ultrasonicated for 1h to form homogeneous solution. Then, 5 μL ink was pipetted onto the surface of glassy carbon electrode (GCE, 5 mm in diameter) resulting in a total mass loading of ~ 0.05 mg $cm^{-2}{}_{geo}$. The accurate loading of catalysts and elements contents were originated from the ICP-AES results listing in table S1.

Cyclic voltammetry (CV) was conducted in 0.1 M KOH solution with Ar-saturated at a scanning rate of 50 mV s^{-1} from -0.18 V to 0.72 V. The HOR polarization curves were recorded by a rotation disk electrode (RDE) with a rotation speed of 1600 rpm in a H_2-saturated 0.1 M KOH and the potential range is from -0.08 V to 0.72 V at a scanning rate of 10 mV s^{-1}.

The HOR polarization under the rotation speed of 2500, 2025, 1600, 1225, 900, and 625 rpm were collected at a scanning rate of 10 mV s^{-1}. The kinetic current density (j^k) of each electrocatalyst could be calculated from the Koutecky-Levich equation (Eq. S1) [1]

$$\frac{1}{j} = \frac{1}{j^k} + \frac{1}{j^d} = \frac{1}{j^k} + \frac{1}{Bc_0\omega^{1/2}} \qquad \text{...........Eq. S1}$$

where j and j^d are the measured and diffusion limited current density, and B represents the Levich constant, c_0 represents the solubility of H_2 (7.33×10^{-4} mol L^{-1}), ω is the rotating speed. Among them, B could be obtained from Eq. S2

$$B = 0.2nFD^{2/3}v^{-1/6} \qquad \text{........... Eq. S2}$$

where n is the numbers of electron transferred, F is the Faraday constant (96485 C mol^{-1}), D is the diffusivity of H_2 (3.7×10^{-5} cm^2 s^{-1}), and v represents the kinematic viscosity (1.01×10^{-2} cm^2 s^{-1}). [2]

Exchange current density (j^0) could be deduced from the Butler–Volmer equation in Eq. S3,

$$j^k = j^0[e^{\frac{\alpha F}{RT}\eta} - e^{\frac{-(1-\alpha)F}{RT}\eta}] \qquad \text{...........Eq. S3}$$

where α is the transfer coefficient, R represents the universal gas constant (8.314 J mol^{-1} K^{-1}), T stands the operating temperature (303.15 K), η is the overpotential. [3]

For Ru-based catalysts, the hydrogen underpotential deposition (H-UPD) method is unsuitable for confirming the electrochemically active surface areas (ECSAs) owing to the adsorption of OH* in H-UPD area. [4] Correspondingly, the Cu-UPD method is employed to determine the ECSA for the catalysts. The catalysts modified electrode were cycled between 0.20 and 0.70 V in Ar-saturated solution of 0.1 M H_2SO_4 with 2 mM $CuSO_4$ to obtain a complete CV containing the UPD and overpotential deposition (OPD) of Cu. Since the stripping peaks of Cu-UPD and Cu-OPD are recorded separately, after eliminated the effect of Cu-OPD in the manner of performing the CV from 0.25 V, the region of Cu-UPD is used to calculate the ECSA. Before the deposition fo Cu, the modified electrodes were cycled between 0 and 0.70 V in pure 0.1 M H_2SO_4 as the background. The surface charge density of 420 μC cm^{-2} is assigned as a monolayer adsorption of Cu on catalysts. All the values of ECSAs are exhibited in Table S2. The value of ECSAs could be calculated via Eq. S4:

$$\text{ECSA}\left(\frac{cm_{metal}^2}{g_{metal}}\right) = \frac{Q_{Cu}}{M_{metal}\, 420C\; cm^{-2}} \qquad \text{...........Eq. S4}$$

where M_{metal} is the mass loading of metals on the electrode.

For the CO stripping experiments, the samples were kept at 0.1 V versus RHE for 10 min in the saturated CO to adsorb CO on the metal surface, [5] followed by pumping Ar for 20 min to remove residual CO in the electrolyte. The CO stripping current was collected through cyclic voltammetry in a potential range from 0 to 0.9 V at a scanning rate of 5 mV s^{-1}.

The stability of catalyst was appraised by the accelerated durability tests by scanning the potential between -0.08 and 0.72 V for 1000 cycles at the scanning rate of 500 mV s^{-1}. Then, the HOR polarization curve was recorded in H_2-saturated 0.1 M KOH electrolyte at 10 mV s^{-1} from 0.92 to -0.08 V via the comparison with the initial curve. The loading of catalyst is around 30 μg cm$_{disc}^{-2}$.

For HER experiments, the mixture solvent containing 5 mg catalysts and 1 ml isopropanol solution containing 0.05% Nafion was ultrasonicated for 1h, forming homogeneous solution. 6 μL dispersion was loaded on the surface of GCE leading a catalyst loading of ~ 0.15 mg cm^{-2} $_{geo}$. HER tests were performed in Ar-saturated 0.1 M KOH and 1.0 M KOH solution (vs. RHE) at 10 mV s^{-1} with a rotation speed of 1700 rpm.

In this work, all the potentials in HOR and HER tests were referred to reversible hydrogen electrode (RHE) with *i*R-compensation. The uncompensated resistance (R_u) was measured by the electrochemical impedance spectra (EIS) tests. EIS tests were measured from 200 kHz to 0.1 kHz at a voltage perturbation of 5 mV after each RDE measurement. The iR-free potential ($E_{iR\text{-}free}$) was obtained by using the value of the real part of the resistance at 1 kHz, according to the following equation, Eq. S5,

$$E_{iR-free} = E - iR_u \qquad \text{Eq. S5}$$

where E, i are the measured potential and the corresponding current.

Computational methods

Density functional theory (DFT) with the Perdew-Burke-Ernzerhof (PBE) and generalized gradient corrected approximation (GGA) was carried out for electronic structure calculations. [6-7] The cutoff energy was 400 eV and the self-consistent field (SCF) tolerance was 1×10^{-5} eV. The Brillouin zone was sampled by the Monkhorst-Pack scheme with a 4×4×1 k-points mesh for all of the surfaces. The four-layers of Ru (001) surface were modelled with 4*4 supercell and a vacuum width of 15 Å was added in the z axis. For all the optimization calculations, the bottom two layers were fixed while the topmost two layers and the adsorbates were allowed to relax. The binding energies of H* were determined by the following formula $\Delta E_{H^*} = E(\text{surf} + \text{H}) - E(\text{surf}) - 1/2E(\text{H}_2)$. The binding energies of OH* were determined by the following formula $\Delta E_{OH^*} = E(\text{surf} + \text{OH}) - E(\text{surf}) - E(\text{H}_2\text{O}) + 1/2E(\text{H}_2)$.

$E_{sub\text{-}H}$ and $E_{sub\text{-}OH}$ represent total energies of the model with hydrogen and hydroxyl adsorption. E_{sub} represents total energy of the model. E_{H2} and E_{H2O} represent the energy of molecular H_2 and H_2O in gas phase.

The Gibbs free energy of H* adsorption was calculated as follows:

$\Delta G_{H^*} = \Delta E_{H^*} + \Delta ZPE - T\Delta S$

ΔZPE and ΔS represent the zero point energy correction and entropy change of hydrogen adsorption, respectively. And We refer to the previous work for the related values. [8]

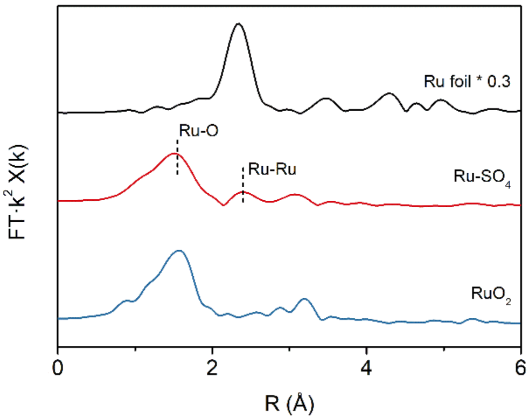

Figure S1 FT k^2 -weighted- EXAFS spectra of Ru foil and Ru-SO$_4$.

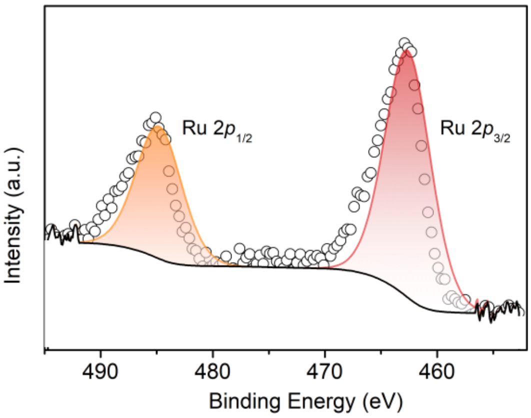

Figure S2 XPS spectra of Ru 3*p* for Ru-SO$_4$.

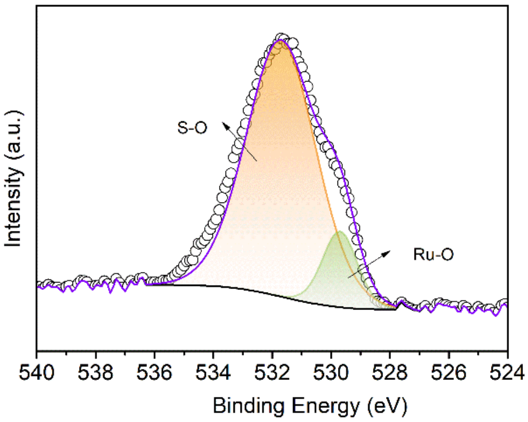

Figure S3 XPS spectra of O 1*s* for Ru-SO$_4$.

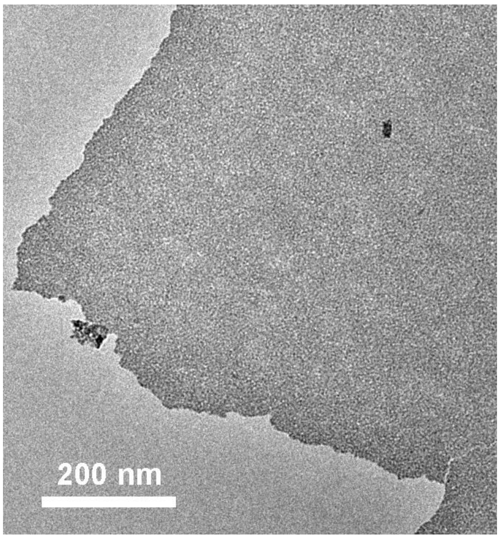

Figure S4 TEM image of Ru.

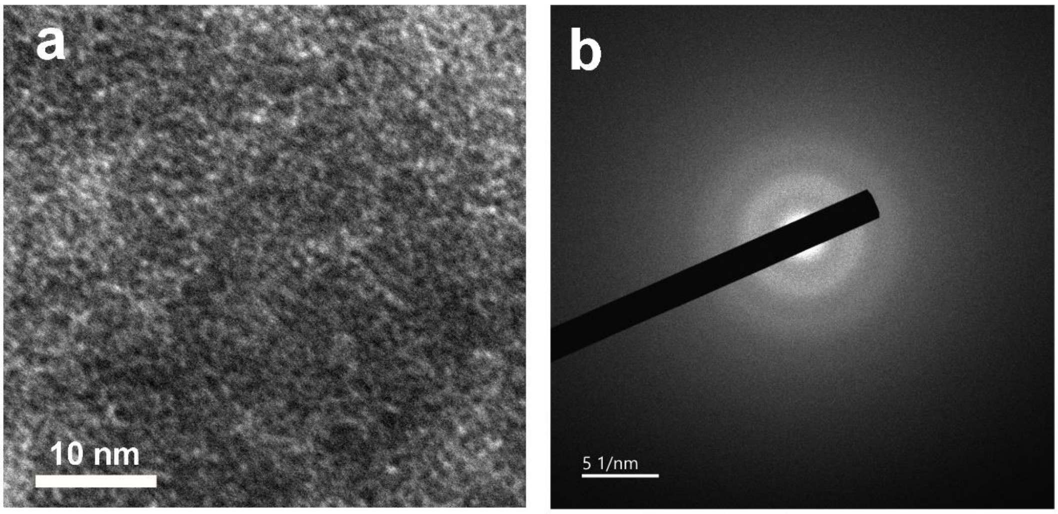

Figure S5 HR-TEM(a) and SAED pattern image(b) of Ru.

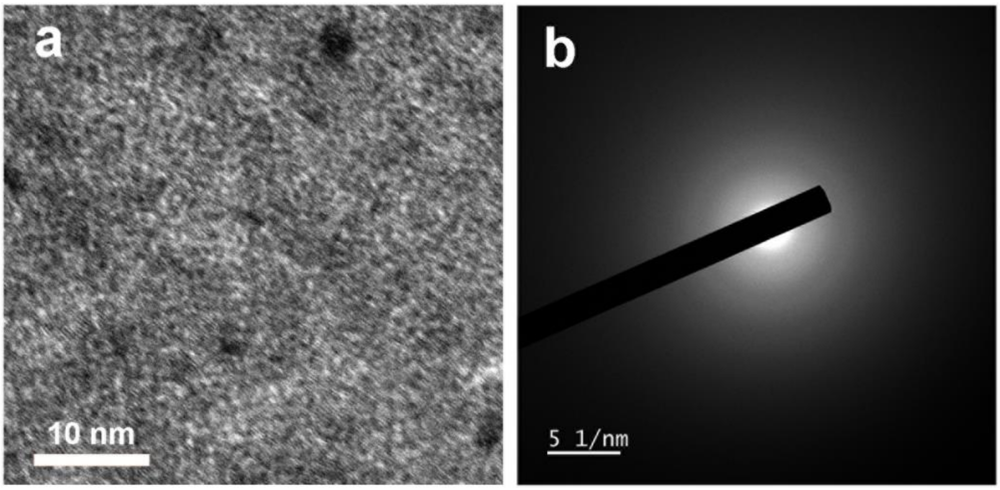

Figure S6 HR-TEM(a) and SAED pattern image(b) of Ru-SO_4.

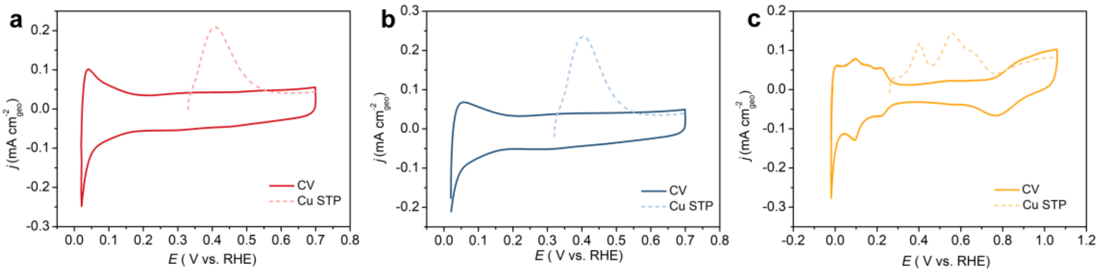

Figure S7 The CV curves of Ru-SO_4 (a), Ru (b) and Pt (c) as well as the Cu-UPD zones.

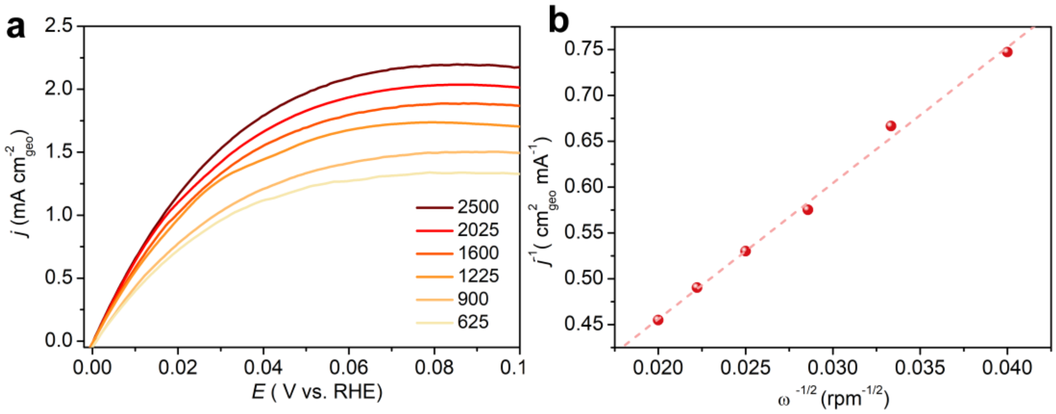

Figure S8 Polarization curves of Ru-SO_4(a) in H_2-saturated 0.1 M KOH solution at the rotating speeds varied from 2500 to 625 rpm. And the Koutecky–Levich plot of Ru-SO_4(b).

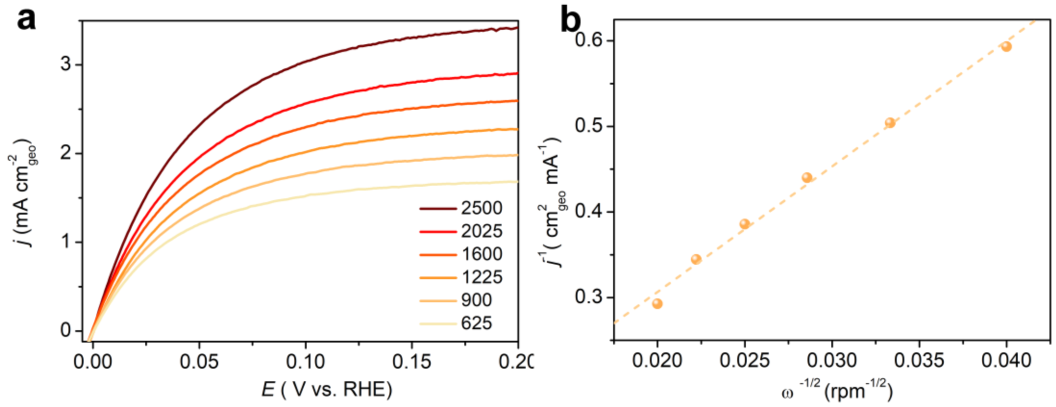

Figure S9. Polarization curves of Pt(a) in H_2-saturated 0.1 M KOH solution at the rotating speeds varied from 2500 to 625 rpm. And the Koutecky–Levich plot of Pt(b).

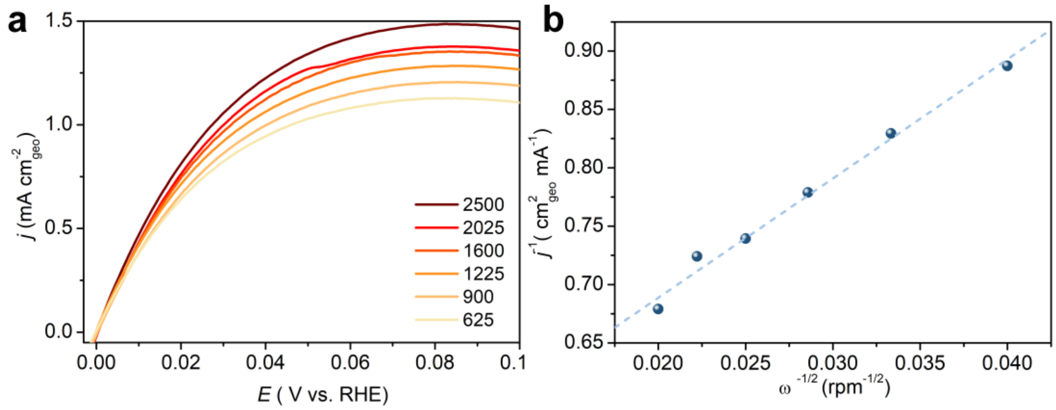

Figure S10. Polarization curves of Ru(a) in H_2-saturated 0.1 M KOH solution at the rotating speeds varied from 2500 to 625 rpm. And the Koutecky–Levich plot of Ru(b).

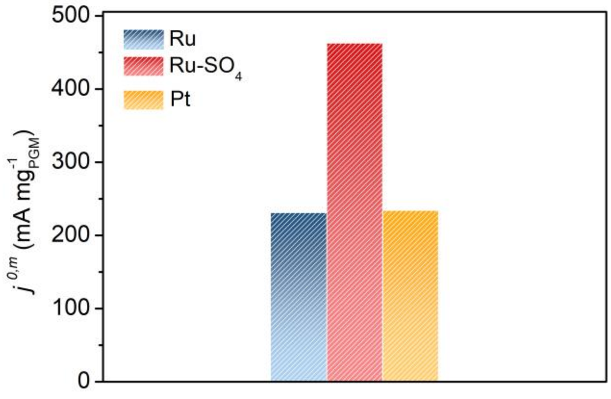

Figure S11. Exchange current densities normalized by corresponding metal mass of Ru-SO_4, Ru and Pt.

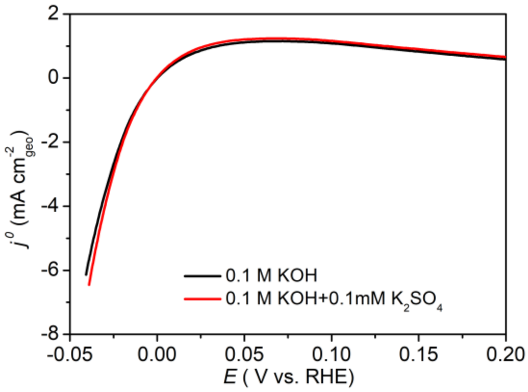

Figure S12 The HOR polarization curves of Ru in 0.1M KOH and Ru in 0.1M KOH with 0.1 mM K_2SO_4.

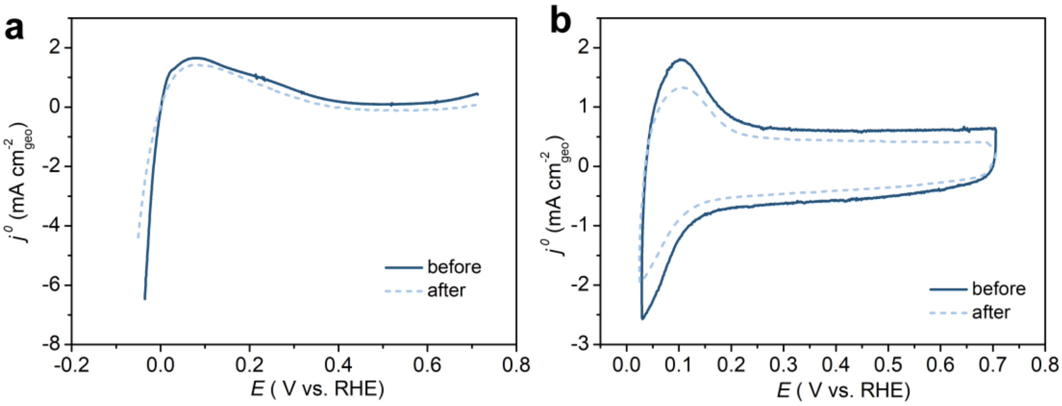

Figure S13 Electrochemical stability tests of Ru. (a) HOR polarization curves in H_2-saturated 0.1 M KOH at a rotating speed of 1600 rpm before and after 1000 CVs. (b) CVs in Ar-saturated 0.1 M KOH before and after 1000 CVs.

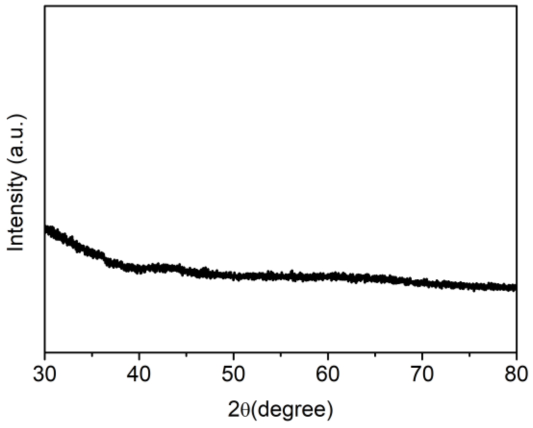

Figure S14 XRD pattern of Ru-SO_4 after HOR stability test in 0.1 M KOH solution.

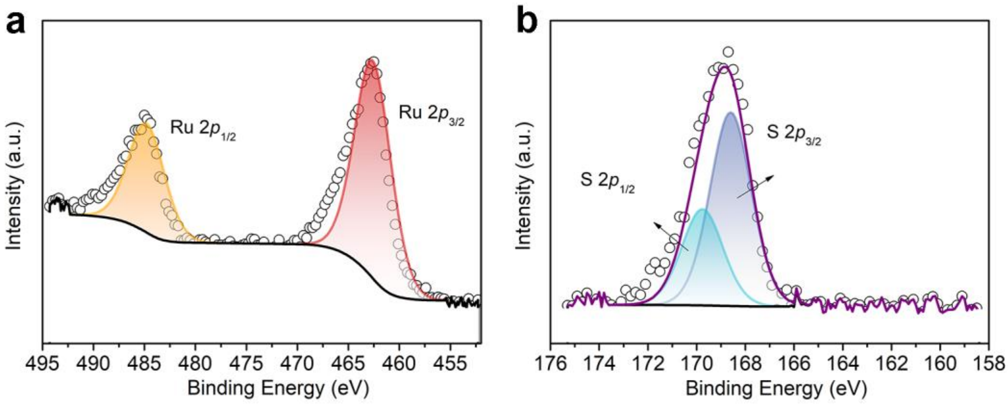

Figure S15 XPS pattern of Ru-SO_4 after HOR stability test in 0.1 M KOH solution.

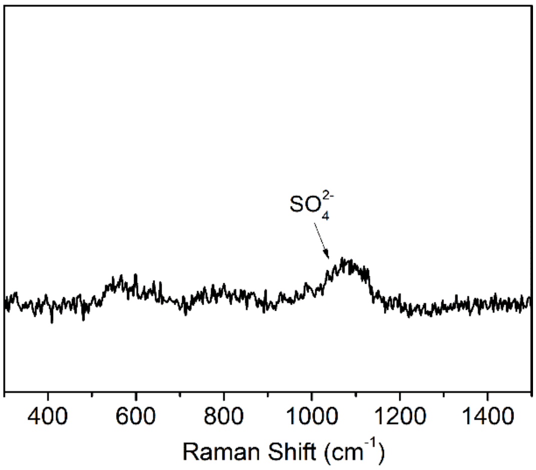

Figure S16 The Raman spectra for Ru-SO_4 after HOR stability test in 0.1M KOH solution.

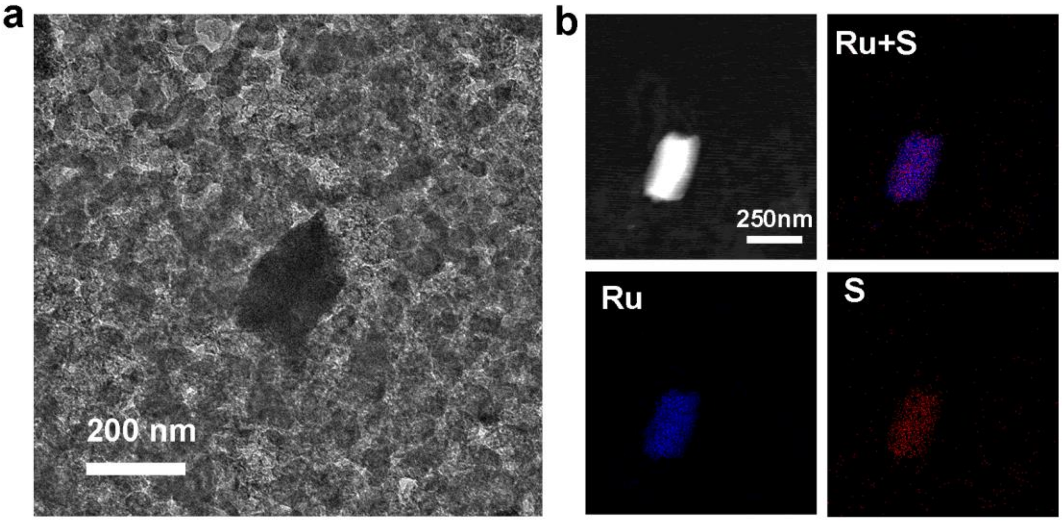

Figure S17 (a) The TEM image and (b) the EDX mapping images for Ru-SO_4 after

HOR stability test in 0.1M KOH solution.

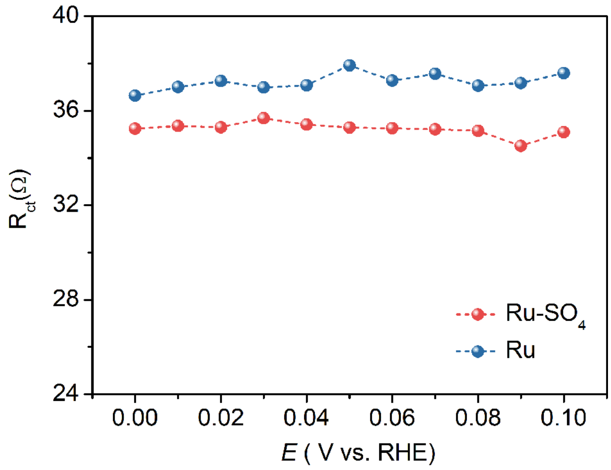

Figure S18 R_{ct} of Ru-SO$_4$ and Ru under different potentials.

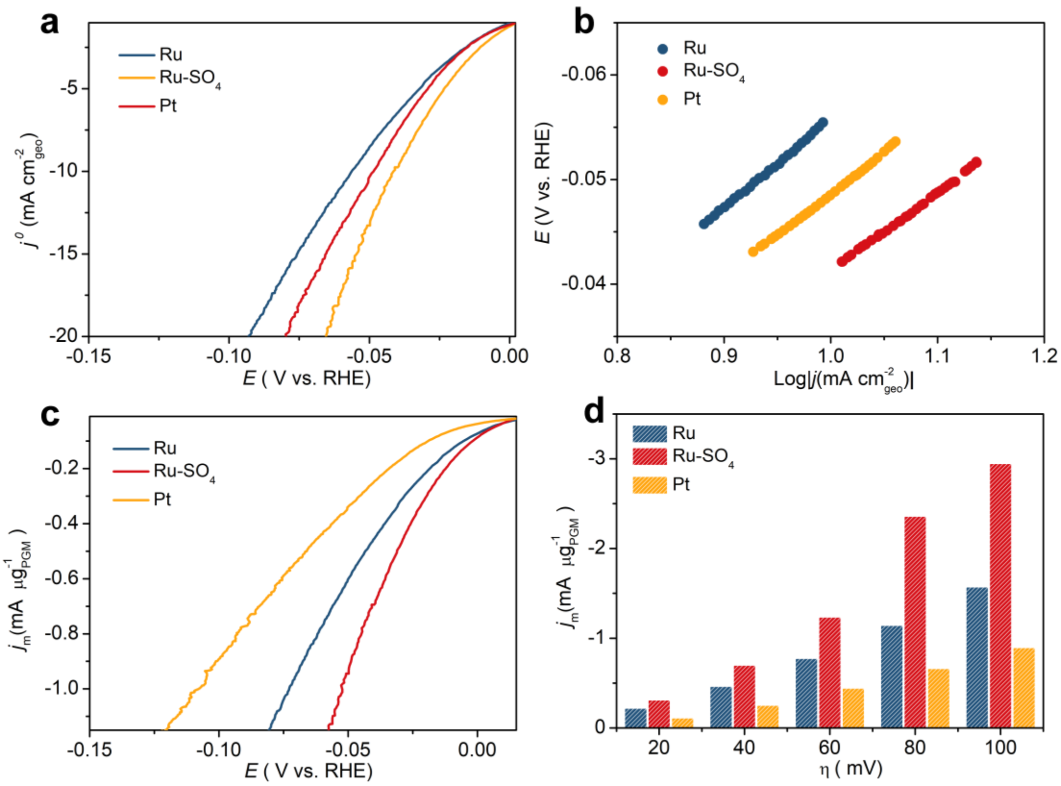

Figure S19 (a) HER polarization curves of Ru-SO$_4$, Ru and Pt catalysts in 0.1M KOH. (b) The corresponding Tafel plots. (c, d) HER polarization curves and the corresponding exchange current density at different overpotentials of Ru-SO$_4$, Ru and Pt catalysts in 0.1 M KOH normalized with the mass of noble metal calculated by ICP-AES.

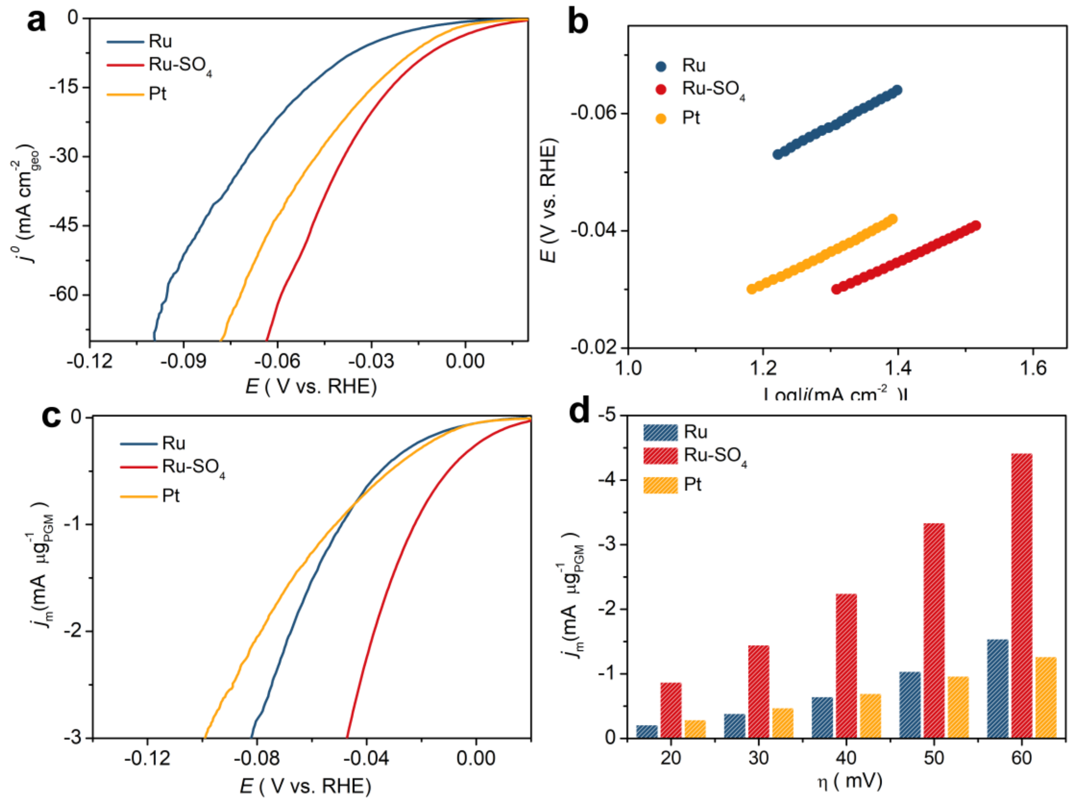

Figure S20 (a) HER polarization curves of Ru-SO_4, Ru and Pt catalysts in 1M KOH. (b) The corresponding Tafel plots. (c, d) HER polarization curves and the corresponding exchange current density at different overpotentials of Ru-SO_4, Ru and Pt catalysts in 1 M KOH normalized with the mass of noble metal calculated by ICP-AES.

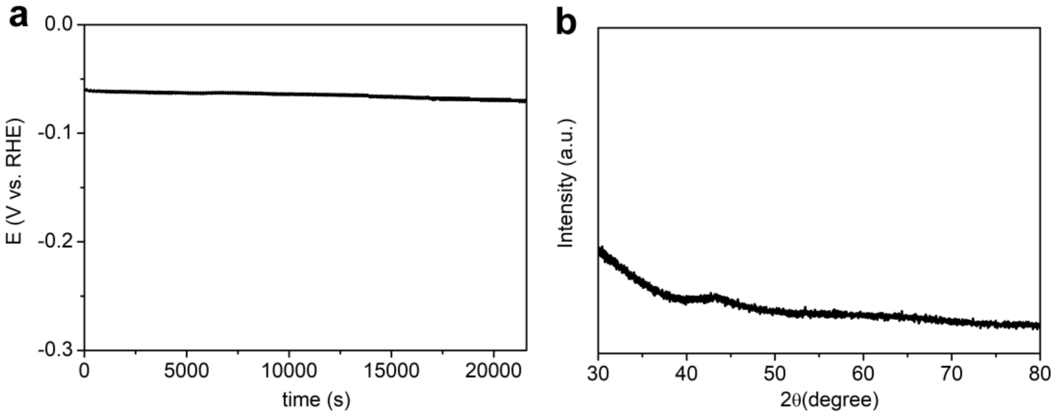

Figure S21 (a) Chronopotentiometric measurement of the HER at 10 mA cm^{-2} using Ru-SO_4 as a catalyst in 0.1 M KOH. (b) XRD pattern of Ru-SO_4 after HER stability.

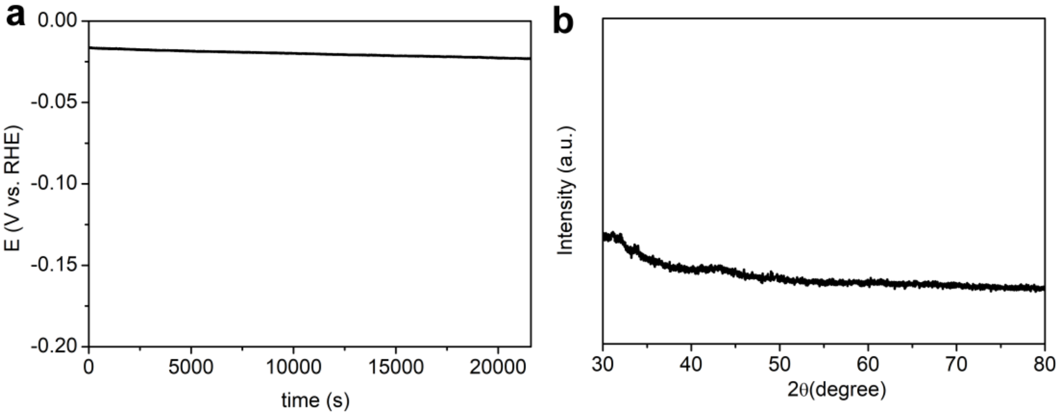

Figure S22 (a) Chronopotentiometric measurement of the HER at 10 mA cm^{-2} using Ru-SO_4 as a catalyst in 1 M KOH. (b) XRD pattern of Ru-SO_4 after HER stability.

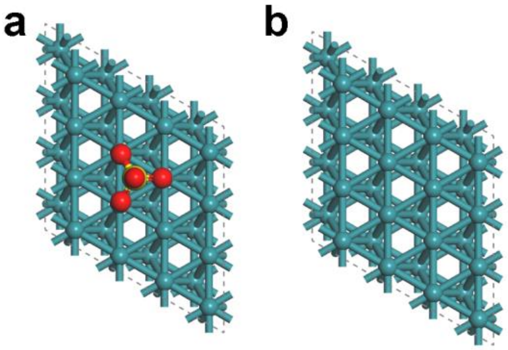

Figure S23 The geometric configurations of Ru-SO_4 (a) and Ru(b).

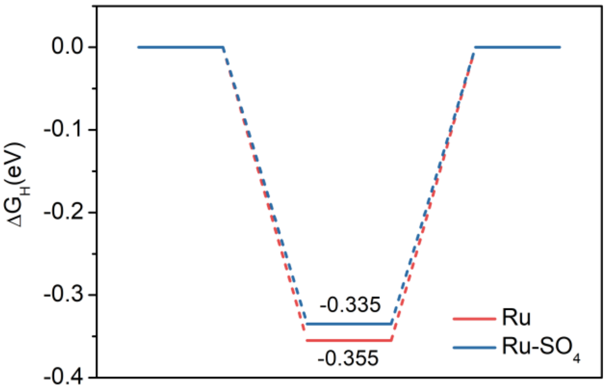

Figure S24 HBE of Ru-SO_4 and Ru.

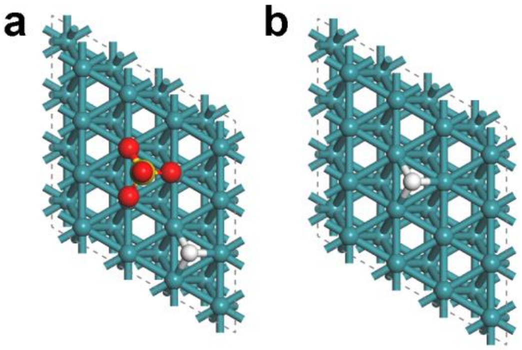

Figure S25 The optimal theoretical structures of H* on Ru-SO_4 (a) and Ru (b).

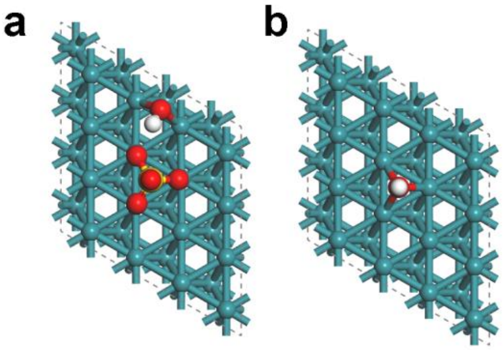

Figure S26 The optimal theoretical structures of OH* on Ru-SO_4 (a) and Ru (b).

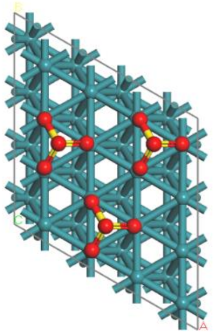

Figure S27 The geometric configurations of Ru-SO_4-2.

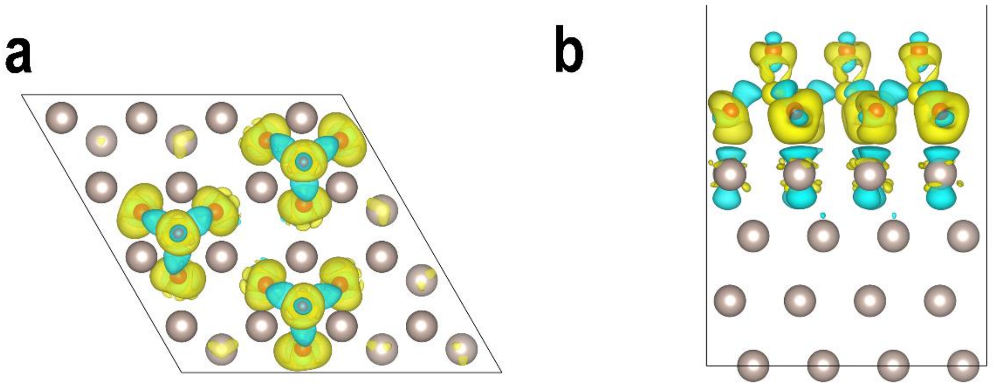

Figure S28 Calculated differential charge density for Ru-SO_4-2 of top view (a) and side view(b). The blue and yellow areas correspond to the depletion and accumulation of electrons, respectively.

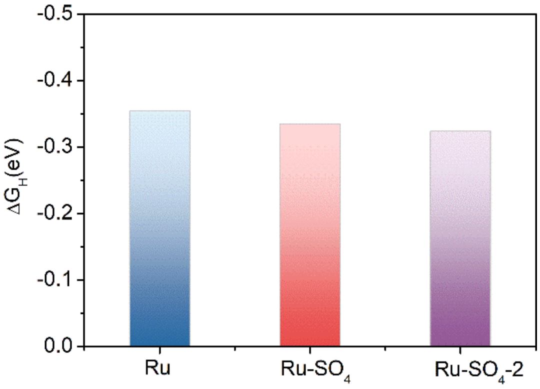

Figure S29 ΔG_H of Ru, Ru-SO_4 and Ru-SO_4-2.

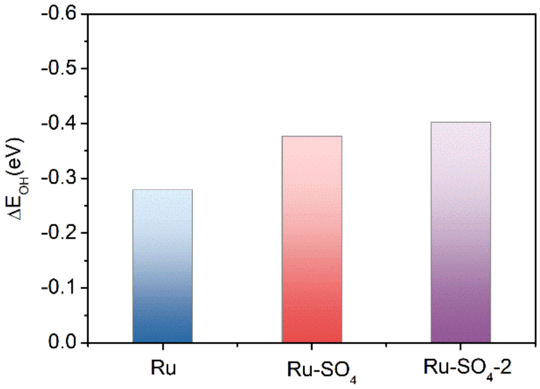

Figure S30 OHBE of Ru, Ru-SO_4 and Ru-SO_4-2.

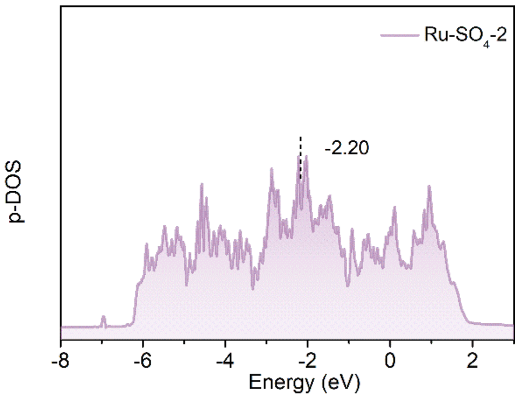

Figure S31 The projected density of states of Ru-SO_4-2.

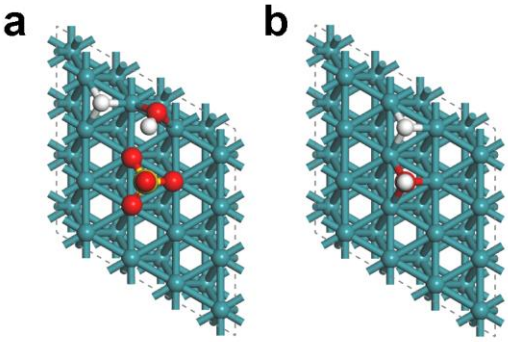

Figure S32 The optimal theoretical structures of OH*+H* on Ru-SO_4 (a) and Ru (b).

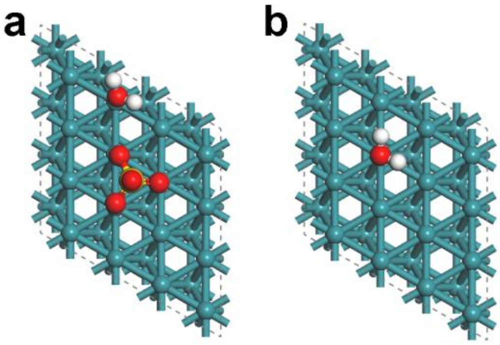

Figure S33 The optimal theoretical structures of H_2O on Ru-SO_4 (a) and Ru (b).

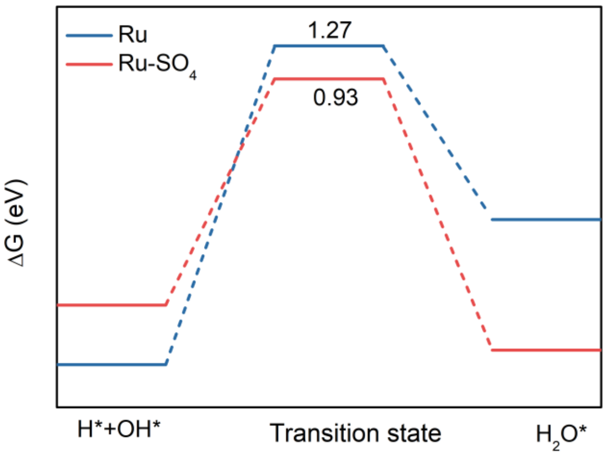

Figure S34 Calculated activation energy of water formation on Ru-SO$_4$ and Ru.

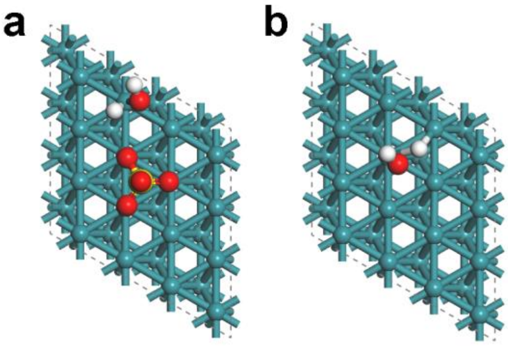

Figure S35 Theoretical structures transition state (OH-H)* of Ru-SO$_4$ (a) and Ru (b).

Table S1 ICP-AES results of the contents of S and Ru in different catalysts.

Catalyst	**S (wt. %)**	**SO_4^{2-} ion (wt. %)**	**Ru (wt. %)**
Ru-SO$_4$/C	1.25	3.75	9.38
Ru/C	-	-	9.29

Table S2. HOR activities of the reported PGM-based catalysts in alkaline media.

Catalyst	**Loading (μg_{PGM} cm^{-2})**	**$j^{0,s}$ (mA cm$_{metal}^{-2}$)**	**$j^{k,m}$ (mA μg_{metal}^{-1})**	**Reference**
Ru-SO$_4$	4.78	0.548	1.182	This work
Ru/C (3.1 nm)	10	0.063	0.082	4
Pt$_7$Ru$_3$ NWs	~20	0.493	0.600	9
Pt$_7$Fe$_3$ NWs	~20	0.459	/	9
Pt$_7$Co$_3$ NWs	~20	0.394	/	9

Ru/Meso C	25.4	/	0.54	10
Ru-TiO_2/C	25.48	0.15	0.097	11
Ru/C	25.48	0.12	0.052	11
$Ru_{0.7}Ni_{0.3}$/C	14	0.13	0.14	12
$Ru_{0.95}Fe_{0.05}$/C	14	0.11	0.16	12
$(Pt_{0.9}Pd_{0.1})_3Fe$/C	5	0.99	0.330	13
Ru-Ir(2/3)/C	10	0.283	0.210	14
PdCu/C-400℃	1.45	0.356	0.245	15
PdCu/C-500℃	1.69	0.883	0.522	15
$Pd_{0.33}Ir_{0.67}$/N-C	10	0.45	0.481	16
RuRh-Co	250	/	0.011	17
PtRu/Mo_2C-TaC	13	0.2	0.291	18
PtRh	25.5	0.34	0.322	19
Ru colloidosomes	57	0.045	/	20
D-PdFe@Pt/C	5	0.076	0.077	21
O-PdFe@Pt/C	5	0.243	0.248	21
Rh NBs	10	0.146	0.361	22
Rh NP/PC	54.8	0.164	0.163	23
Ru NP/PC	50.1	0.227	0.263	23
Ni_1Ru_1/C	12.5	0.078	0.224	24

Table S3. Summary of the mass activities ($j_{0,m}$) of the catalysts in this work.

Sample	**$j_{0,m}$ (mA mg_{PGM}^{-1})**
Ru-SO_4	462.54
Ru	230.69
Pt	234.29

Table S4. Comparison of HER activities for precious metal based electrocatalysts in pH-universal electrolytes.

Catalysts	**Loading (μg cm^{-2})**	**Electrolytes**	**Current density (mA cm^{-2})**	**η (mV)**	**Reference**
Ru-SO_4	14.34	0.1M KOH 1M KOH	10	41.77 16.86	This work
Ru_3Ni_7 NAs	20.4	0.1M KOH 1M KOH	10	119 39	25
NiFe@Pt	/	0.1M KOH	10	70	26
RuCoP	300	1M KOH	10	23	27
$NiRu_{0.13}$-BDC	250	1M KOH	10	34	28
ECM@Ru	300	1M KOH	10	83	29
Ru@GnP	250	1M KOH	10	140	30
Ru/OMSNNC	400	1M KOH	10	13	31
Ru/Co_3O_4 NWs	354	1M KOH	10	31	32
Ru_2Ni_2 SNs/C	100	0.1M KOH 1M KOH	10	39.3 40	33
Ru_1CoP/CDs	/	1M KOH	10	51	34
Ni5P4-Ru/CC	152	1M KOH	10	54	35
Ru/Co–N–C	400	1M KOH	10	23	36
RuCo	153	1M KOH	10	40	37
Ru/rGO-700	255	1M KOH	10	26	38
Pd_3Ru	51.02	1M KOH	10	42	39

References

1. W. C. Sheng, H. A. Gasteiger and Y. Shao-Horn, *J. Electrochem. Soc.*, 2010, **157**, B1529-B1536.
2. J. Zheng, Z. Zhuang, B. Xu and Y. Yan, *ACS Catal.*, 2015, **5**, 4449-4455.
3. J. Durst, A. Siebel, C. Simon, F. Hasché, J. Herranz and H. A. Gasteiger, *Energy Environ. Sci.*, 2014, **7**, 2255-2260.
4. J. Ohyama, T. Sato, Y. Yamamoto, S. Arai and A. Satsuma, *J Am Chem Soc*, 2013, **135**, 8016-8021.
5. Y. Duan, Z. Y. Yu, L. Yang, L. R. Zheng, C. T. Zhang, X. T. Yang, F. Y. Gao, X. L. Zhang, X. Yu, R. Liu, H. H. Ding, C. Gu, X. S. Zheng, L. Shi, J. Jiang, J. F. Zhu, M. R. Gao and S. H. Yu, *Nat. Commun.*, 2020, **11**, 4789.
6. J. P. Perdew, K. Burke and M. Ernzerhof, *Phys. Rev. Lett.*, 1997, **78**, 1396-1396.
7. B. Hammer, L. B. Hansen and J. K. Norskov, *Phys. Rev. B*, 1999, **59**, 7413-7421.
8. J. K. Norskov, T. Bligaard, A. Logadottir, J. R. Kitchin, J. G. Chen, S. Pandelov and J. K. Norskov, *J. Electrochem. Soc.*, 2005, **152**, J23-J26.
9. M. E. Scofield, Y. Zhou, S. Yue, L. Wang, D. Su, X. Tong, M. B. Vukmirovic, R. R. Adzic and S. S. Wong, *ACS Catal.*, 2016, **6**, 3895-3908.
10. J. Jiang, S. Tao, Q. He, J. Wang, Y. Zhou, Z. Xie, W. Ding and Z. Wei, *J. Mater. Chem. A*, 2020, **8**, 10168-10174.
11. L. Zeng, H. Peng, W. Liu, J. Yin, L. Xiao, J. Lu and L. Zhuang, *J. Power Sources*, 2020, **461**, 228147.
12. H. Wang, Y. Yang, F. J. DiSalvo and H. D. Abruña, *ACS Catal.*, 2020, **10**, 4608-4616.
13. T. Zhao, G. Wang, M. Gong, D. Xiao, Y. Chen, T. Shen, Y. Lu, J. Zhang, H. Xin, Q. Li and D. Wang, *ACS Catal.*, 2020, **10**, 15207-15216.
14. K. Ishikawa, J. Ohyama, K. Okubo, K. Murata and A. Satsuma, *ACS Appl Mater Interfaces*, 2020, **12**, 22771-22777.
15. Y. Qiu, L. Xin, Y. Li, I. T. McCrum, F. Guo, T. Ma, Y. Ren, Q. Liu, L. Zhou, S. Gu, M. J. Janik and W. Li, *J. Am. Chem. Soc.*, 2018, **140**, 16580-16588.
16. Y. Cong, I. T. McCrum, X. Gao, Y. Lv, S. Miao, Z. Shao, B. Yi, H. Yu, M. J. Janik and Y. Song, *J. Mater. Chem. A*, 2019, **7**, 3161-3169.
17. Y. Cui, Z. Xu, D. Chen, T. Li, H. Yang, X. Mu, X. Gu, H. Zhou, S. Liu and S. Mu, *Nano Energy*, 2021, **90**, 106579.
18. E. R. Hamo, R. K. Singh, J. C. Douglin, S. Chen, M. B. Hassine, E. Carbo-Argibay, S. Lu, H. Wang, P. J. Ferreira, B. A. Rosen and D. R. Dekel, *ACS Catal.*, 2021, **11**, 932-947.
19. Y. Jin, F. Chen, J. Wang, L. Guo, T. Jin and H. Liu, *J. Power Sources*, 2019, **435**, 226798.
20. X. Yang, B. Ouyang, P. Shen, Y. Sun, Y. Yang, Y. Gao, E. Kan, C. Li, K. Xu and Y. Xie, *J. Am. Chem. Soc.*, 2022, **144**, 11138-11147.
21. W. Xiao, W. Lei, J. Wang, G. Gao, T. Zhao, M. A. L. Cordeiro, R. Lin, M. Gong, X. Guo, E. Stavitski, H. L. Xin, Y. Zhu and D. Wang, *J. Mater. Chem. A*, 2018, **6**, 11346-11352.

22. J. Jiang, S. Tao, Q. He, J. Wang, Y. Zhou, Z. Xie, W. Ding and Z. Wei, *J. Mater. Chem. A*, 2020, **8**, 10168-10174.
23. M. Ming, Y. Zhang, C. He, L. Zhao, S. Niu, G. Fan and J. S. Hu, *Small*, 2019, **15**, e1903057.
24. J. Liu, J. Wang, Y. Fo, B. Zhang, C. Molochas, J. Gao, W. Li, X. Cui, X. Zhou, L. Jiang and P. Tsiakaras, *Chem. Eng. J.*, 2023, **454**, 139959.
25. Y. Cui, Z. Xu, D. Chen, T. Li, H. Yang, X. Mu, X. Gu, H. Zhou, S. Liu, S. Mu, *Nano Energy*, 2021, **90**, 106579.
26. E. R. Hamo, R. K. Singh, J. C. Douglin, S. Chen, M. B. Hassine, E. Carbo-Argibay, S. Lu, H. Wang, P. J. Ferreira, B. A. Rosen, D. R Dekel, *ACS Catal.* 2021, **11**, 932-947.
27. J. Xu, T. Liu, J. Li, B. Li, Y. Liu, B. Zhang, D. Xiong, I. Amorim, W. Li, L. Liu, *Energy Environ. Sci.*, 2018, **11**, 1819-1827.
28. Y. Sun, Z. Xue, Q. Liu, Y. Jia, Y. Li, K. Liu, Y. Lin, M. Liu, G. Li, C. Y. Su, *Nat. Commun.*, 2021, **12**, 1369.
29. H. Zhang, W. Zhou, X. F. Lu, T. Chen, X. W. Lou, *Adv. Energy Mater.*, 2020, **10**, 2000882.
30. F. Li, G. F. Han, H. J. Noh, I. Ahmad, I. Y. Jeon, J. B. Baek, *Adv. Mater.*, 2018, **30**, e1803676.
31. Y. L. Wu, X. Li, Y. S. Wei, Z. Fu, W. Wei, X. T. Wu, Q. L. Zhu, Q. Xu, *Adv. Mater.*, 2021, **33**, 2006965.
32. Z. Liu, L. Zeng, J. Yu, L. Yang, J. Zhang, X. Zhang, F. Han, L. Zhao, X. Li, H. Liu, W. Zhou, *Nano Energy*, 2021, **85**, 105940.
33. J. Ding, Q. Shao, Y. Feng, X. Huang, *Nano Energy*, 2018, **47**, 1-7.
34. H. Song, M. Wu, Z. Tang, J. S. Tse, B. Yang, S. Lu, *Angew. Chem. Int.*, 2021, **60**, 7234-7244.
35. Q. He, D. Tian, H. Jiang, D. Cao, S. Wei, D. Liu, P. Song, Y. Lin, L. Song, *Adv. Mater.*, 2020, **32**, e1906972.
36. C. L. Rong, X. J. Shen, Y. Wang, L. Thomsen, T. W. Zhao, Y. B. Li, X. Y. Lu, R. Amal, C. Zhao, *Adv. Mater.*, 2022, **34**, 2110103.
37. J. Mao, C. T. He, J. Pei, W. Chen, D. He, Y. He, Z. Zhuang, C. Chen, Q. Peng, D. Wang, Y. Li, *Nat. Commun.*, 2018, **9**, 4958.
38. Y. J. Yang, D. X. Wu, Y. H. Yu, J. Li, P. Rao, C. M. Jia, Z. X. Liu, Q. Chen, W. Huang, J. M. Luo, P. L. Deng, Y. J. Shen, X. L. Tian, *Chem. Eng. J.*, 2022, **433**, 134421.
39. X. Qin, L. Zhang, G.-L. Xu, S. Zhu, Q. Wang, M. Gu, X. Zhang, C. Sun, P. B. Balbuena, K. Amine, M. Shao, *ACS Catal.*, **2019**, 9, 9614-9621.